

## MIT Open Access Articles

*Additive Manufacturing Along Principal Stress Lines*

The MIT Faculty has made this article openly available. **Please share** how this access benefits you. Your story matters.

**Citation:** Tam, Kam-Ming Mark and Caitlin T. Mueller. "Additive Manufacturing Along Principal Stress Lines." 3D Printing and Additive Manufacturing 4, 2 (June 2017): 63–81 © 2017 Mary Ann Liebert, Inc

**As Published:** <http://dx.doi.org/10.1089/3DP.2017.0001>

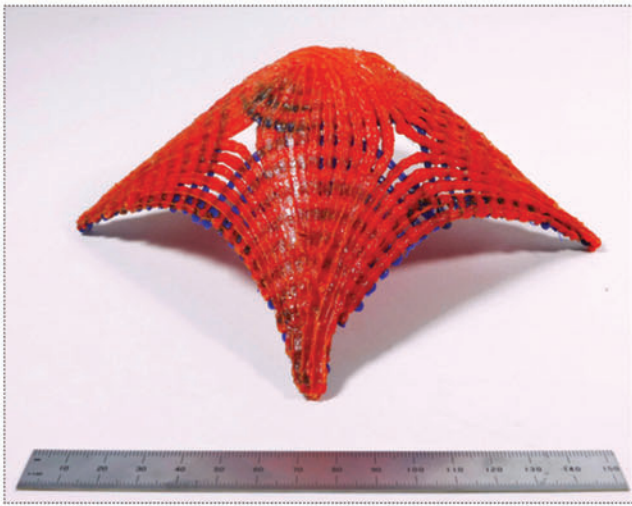
**Publisher:** Mary Ann Liebert Inc

**Persistent URL:** <http://hdl.handle.net/1721.1/116338>

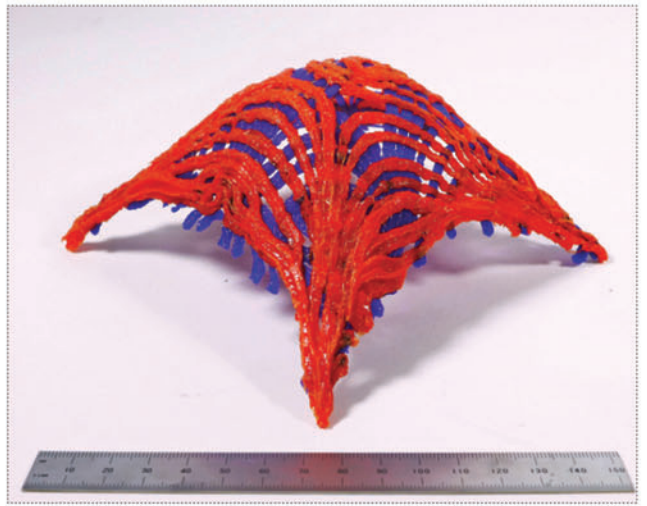
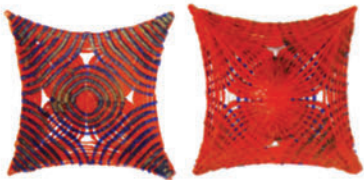
**Version:** Final published version: final published article, as it appeared in a journal, conference proceedings, or other formally published context

**Terms of Use:** Article is made available in accordance with the publisher's policy and may be subject to US copyright law. Please refer to the publisher's site for terms of use.

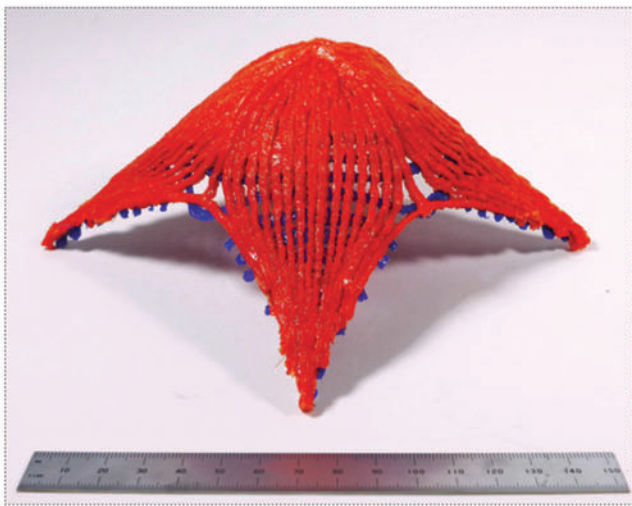
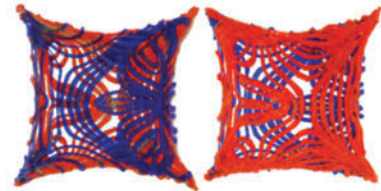




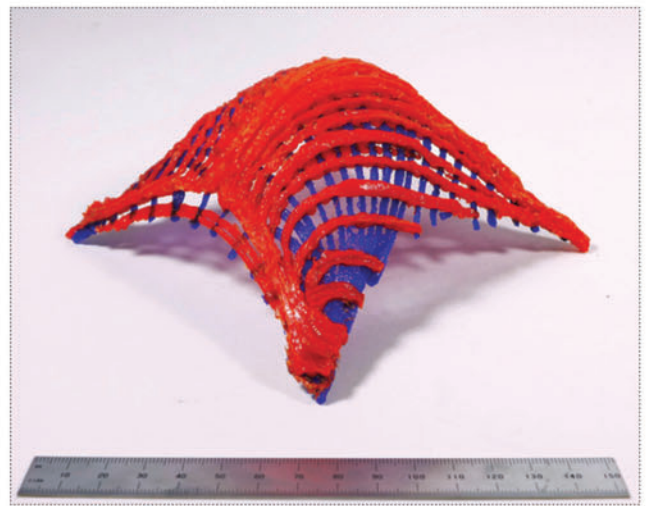
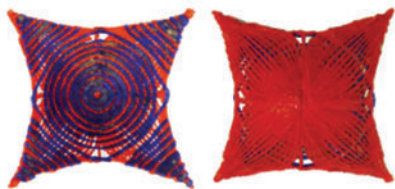
*SL-DL Distributed Loading*



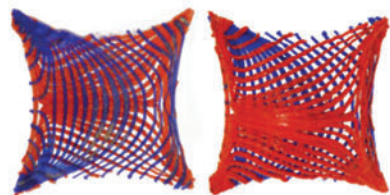
*SL-ADL Asymmetrically Distributed Loading*



*SL-PL Point Loading*



*SL-LL Lateral Loading*



ORIGINAL ARTICLE

# Additive Manufacturing Along Principal Stress Lines

Kam-Ming Mark Tam and Caitlin T. Mueller

## Abstract

Optimization techniques developed for additive manufacturing (AM) to maximize the structural stiffness of printed parts are often computationally expensive reformulations of classical procedures that do not typically consider the mechanical behavior introduced to the printed part by the AM fabrication process, which is layer-based, and result in pieces with significant anisotropy. The misalignment of filament orientation and structural action negates the potential benefits of optimization. Addressing this problem, this article presents a two-part research approach exploring a new method of material deposition called Stress Line Additive Manufacturing (SLAM), which deposits filament along paths derived from principal stress lines. The proposed method unifies the design and optimization of the geometry and filament layout of AM-produced parts, and is compatible to the operational characteristics of fused deposition modeling (FDM). Experimentally validating the structural significance of oriented filament, the first part of the research implements SLAM on a commercial platform for planar design cases. Ongoing research to adapt SLAM for complex 2.5D surface geometries using a six-axis industrial robot arm and a custom-designed heated extruder is then presented in Implementation 2: Robot-Enabled SLAM for 2.5-D Cases. The presented research opens new possibilities for structurally performative fabrication.

**Keywords:** additive manufacturing, anisotropy, fused deposition modeling, principal stress lines, structural optimization, toolpath planning

## Introduction

OFTEN DESCRIBED AS a disruptive technology<sup>1,2</sup> or innovation,<sup>3</sup> additive manufacturing (AM) is characterized by processes that are built up layer-by-layer, in contrast to traditional fabrication methods based on material removal.<sup>4</sup> The manufacturing approach, which has now been applied in the aerospace,<sup>5</sup> automotive,<sup>6</sup> and medical<sup>7</sup> industries, allows parts of greater complexity to be produced without significant effects to costs.<sup>4</sup> For engineers and designers seeking to capitalize the critical relationship between geometry and performance, the potential of the fabrication method, where “complex geometry is no longer a limiting factor,<sup>8,9</sup>” is significant; using AM, it may now be possible to materialize high-performing optimal structures that achieve strength through intelligent, but complex, geometries—structures that were once considered merely theoretical ideals because they were too complicated to be produced.

While AM holds significant promise, a number of mechanical challenges intrinsic to conventional AM fabrication processes and design characterization limit the structural performance and, by extension, the end-use application of AM-produced elements. As Figure 1 illustrates, the design of AM-produced parts can be conceived in three scales: (1) global geometry; (2) topology, or material distribution; and (3) layer pattern, or filament layout. However, current performance-oriented AM design and optimization methods do not simultaneously consider all three scales. These methods largely borrow from earlier techniques based on traditional manufacturing processes; there is a lack of structurally informed methods for incorporating AM-specific manufacturing considerations.<sup>4</sup> Consequently, a general disconnect exists between the design and optimization of the printed element’s global geometry and the printing instructions for the mechanical extrusion process, leading to inconsistent structural behavior at the

Massachusetts Institute of Technology, School of Architecture and Planning, Department of Architecture, Building Technology Program, Cambridge, Massachusetts.

*Opposite page:* To validate the capacity of the robotic adaptation of Stress Line Additive Manufacturing (SLAM) in producing high-performing complex 2.5-D surface geometries, the research presented here generated and fabricated four SLAM specimens based on the stress line information of a form-found four-support gridshell analyzed under various loading conditions. As the figure shows, these load cases include distributed load (labeled SL-DL), point load (SL-PL), asymmetrically distributed load (SL-ADL), and lateral load (SL-LL). Structural load testings were subsequently carried out on SL-DL and SL-PL—showing that the SLAM cases registered improvement in stiffness, ultimate strength capacity and ductility after initial failure in comparison to specimens produced using commercial additive manufacturing platforms. *Photo credit:* Digital Structures.

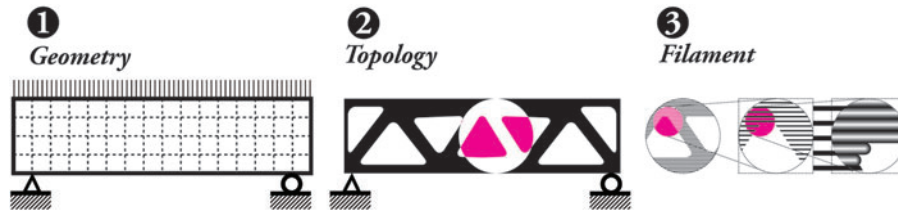


FIG. 1. Design scales for AM-produced parts: (1) global geometry; (2) topology; and (3) filament layout. AM, additive manufacturing.

three scales. The problem is particularly pronounced when anisotropy-causing AM techniques such as fused deposition modeling (FDM) are used.<sup>10</sup> Addressing this gap, this article develops a novel method of structurally informed material deposition compatible with the operational characteristics of FDM called Stress Line Additive Manufacturing (SLAM).

**Literature Review and Related Works**

*Anisotropic limitation and deposition orientation*

The structural challenges of existing AM processes are attributed to the three-axis layer-based paradigm of conven-

tional printing techniques. Anisotropic behavior can be found in parts produced by FDM,<sup>11–15</sup> inkjet three-dimensional (3D) printing,<sup>16,17</sup> and various metal AM systems<sup>18,19</sup>; the problem is especially pronounced for parts fabricated using FDM, which is an AM process that extrudes partially melted thermoplastic filament through a heated nozzle into thin layers on the horizontal build platform in the form of a prescribed two-dimensional (2D) layer pattern.<sup>20</sup> In FDM-produced parts, the strength along filament axes is significantly stronger than the bonding strength between the layers, because the weak fusion between horizontal layers provides a natural point for breakage.<sup>10</sup> (Fig. 2.3). Consequently, the technique leads to

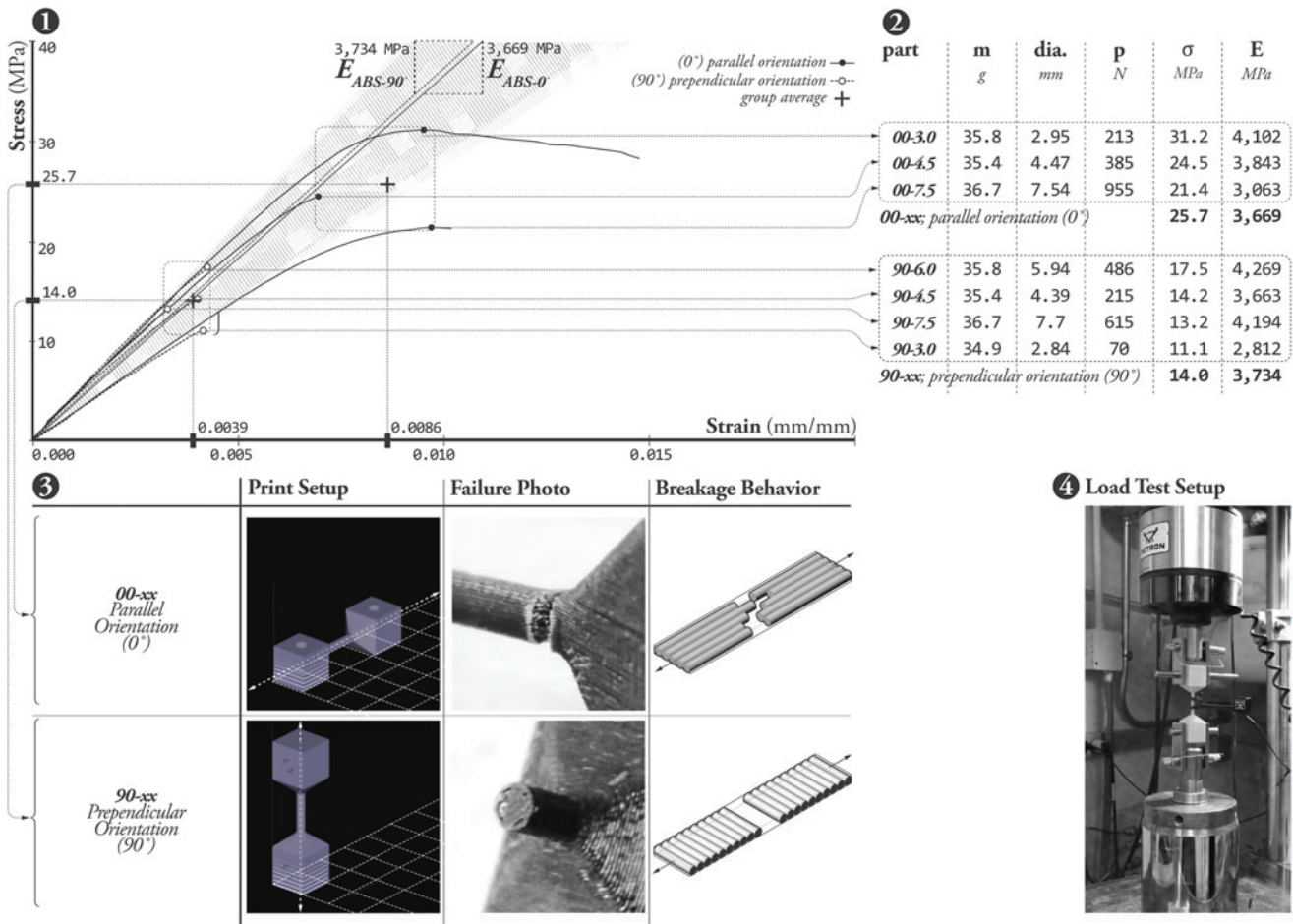


FIG. 2. Experimental testing setup and results of various cylindrical ABS specimens loaded in direct tension: (1) stress-strain plots of seven tested specimens, which are labeled at their ultimate loads; (2) geometry and weight of printed specimens and corresponding load, stress, and elastic modulus results; (3) print setup and failure documentation; and (4) structural load test setup. ABS, acrylonitrile butadiene styrene.

TABLE 1. SUMMARY OF EXPERIMENTAL LOAD TESTING RESULTS BY VARIOUS RESEARCHERS SHOWING ANISOTROPY IN FUSED-DEPOSITION MODELING PRODUCED PARTS

Studies	Material	Normalized tensile strength of parts loaded perpendicularly to filament orientation (%)
Bagsik <i>et al.</i> <sup>11</sup>	ULTEM Resin	64
Rodríguez <i>et al.</i> <sup>12</sup>	ABS	56
Ahn <i>et al.</i> <sup>13</sup>	ABS	57
Ziemian <i>et al.</i> <sup>14</sup>	ABS	56
Results by authors presented above	ABS	55

The percentage figures in the rightmost column indicates the tensile capacity of FDM-produced parts when loaded perpendicular to filament orientation (transverse or out of plane) normalized by the capacity of the parts when loaded parallel to filament orientation (axial or in plane).

ABS, acrylonitrile butadiene styrene; FDM, fused deposition modeling.

anisotropic manufactured parts with strength and ductility properties that vary significantly depending on the orientation of the applied forces. The inconsistent material property reduces the structural strength of the printed object.

As Table 1 shows, numerous researchers have experimentally quantified the anisotropic limitation of FDM-produced parts. Their findings show that the tensile capacity of FDM-produced parts when loaded perpendicular to filament orientation (transverse or out of plane) is between 55% and 64%<sup>11–14</sup> the tensile capacity achievable when load is applied parallel to the print layers (axial or in plane)—depending on the AM technique used. Experiments conducted by the authors also corroborate these findings: Figure 2.1 and 2.2 summarize structural load test results on FDM-produced acrylonitrile butadiene styrene (ABS) plastic in direct tension, showing that the tensile capacity of specimens loaded perpendicular to filament orientation is 45% weaker than a specimen loaded parallel. This anisotropy negatively affects the durability of the printed specimen and limits the end-use application of AM technologies.<sup>21,22</sup>

#### Manufacturability centric AM topology optimization

Despite the well-established documentation of material anisotropy, an assumption of material isotropy is implied in conventional strategies for optimizing geometries to be produced using FDM. As Figure 3 summarizes, AM-oriented optimization strategies are commonly defined along two goals: (1) methods for modifying global geometry to improve structural and fabrication efficiency (Fig. 3.1); and (2) fabrication-efficient methods for decomposing the horizontal layers of a print geometry into the filament layout (Fig. 3.2).

Strategies of the first goal reformulate classical methods used in structural optimization, where the primary objective function is the minimization of strain energy given a fixed material volume, or in other words, the maximization of the structural stiffness-to-weight ratio. For manufacturability and fabrication efficiency, the objective is to minimize the requirement of scaffolding or support structure. The re-

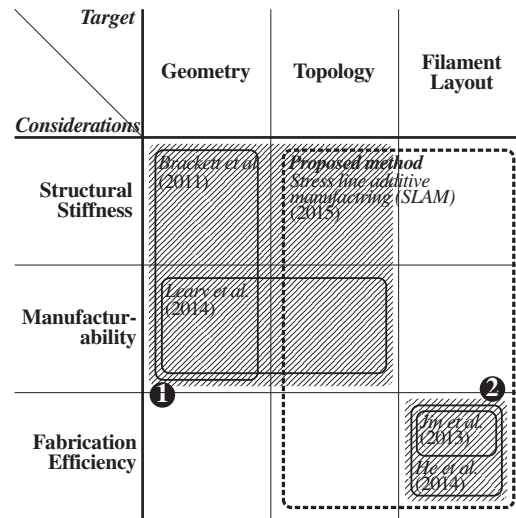


FIG. 3. Diagram mapping current research on AM optimization methods: (1) methods for modifying global geometry to improve structural and fabrication efficiency; and (2) fabrication-efficient methods for decomposing the horizontal layers of a print geometry into the filament layout.

quirement for scaffolding is determined by the interaction of the printed parts' geometry and the technical fabrication constraints of the FDM platform in use, which include the maximum bridging distance and minimum inclination angle of overhanging parts that can be printed without the use of support material.<sup>23,24</sup> Brackett *et al.*'s framework typifies one approach that utilizes single objective design optimization to scalarize structural and fabrication objectives into one weighted sum, adapting a bidirectional evolutionary structural optimization (BESO) to include a penalty function accounting the geometrical features requiring supports.<sup>4</sup> Using similar geometric criteria, Leary *et al.* alternatively proposed a postprocessing strategy that modifies the infeasible geometries of an initially optimized geometry.<sup>25</sup>

In research explicitly considering the filament layout, the objective is to optimize the tool-path planning strategy to improve the precision, surface quality, and strength of prototypes, and reduce the building time and forming material requirements. Tool-path planning encompasses both boundary filling and path sequencing strategies, which, respectively, seek to minimize the number of subpaths required for decomposing a printed geometry, and the nonprinting time expended for relocating the print head to connect discontinuous subpaths. Relevant work in the first category include Jin *et al.*, who proposed a mixed tool-path generation algorithm to hybridize the advantages of the two boundary filling techniques commonly used by today's platform, which include direction-parallel path (DPP; contour-parallel path [CPP]; as illustrated at a later section by Fig. 4.1) and CPP (Fig. 4.2) planning.<sup>26</sup> Expanding on the work, Han *et al.* developed a path optimization framework that additionally optimized the inclination of referenced axis for creating parallel paths, the generation and grouping tool-path segments into individual subpaths, and the linking of subpaths based on specific requirements.<sup>27</sup> Outside of research, developers of commercial platforms have also devised their own proprietary, unpublished algorithms.

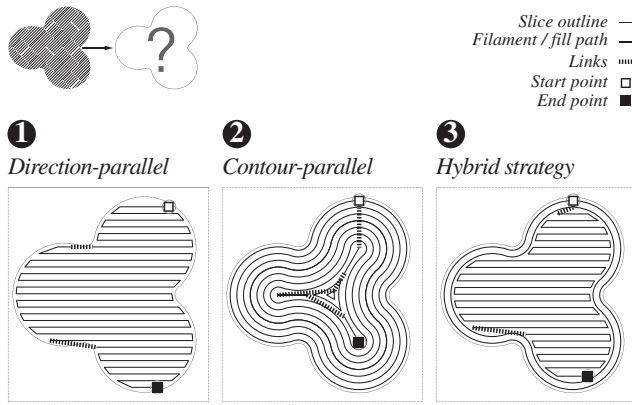


FIG. 4. Conventional tool-path filling techniques: (1) direction-parallel; (2) contour-parallel; and (3) hybrid path planning.

#### Problem statement and article outline

The literature review reveals that AM-specific optimization research is generally agnostic to the extrusion mechanism; the design and optimization of AM-produced parts' global geometry is divorced from the filament layout generated by the tool-pathing strategies that comprise the print geometry. The compartmentalized workflow consists of the following: (1) topology optimization; (2) global geometry processing; and (3) slicing followed by the decomposition of global geometry into tool-paths. Since structural and fabrication objectives are not well integrated in the design generation of the printed part, most approaches require the modification of initially optimized geometries. With structural guidance only utilized in the beginning, the determining role that the filament layout has on both the printed parts' material and global structural performance is ignored, contributing to an inconsistency in structural behavior at the scale of the geometry, topology, and filament layout that negate the potential gains of geometrical optimization. Even in techniques engaging both structural and fabrication objectives, there is a lack of numerical and experimental data to validate the structural performance of design generated using these techniques, or studies of the trade-off in performance between structural stiffness and manufacturability.

Recognizing that the structural challenge intrinsic to existing optimization approaches for AM is primarily caused by poor design-fabrication-performance integration or more precisely, a lack of structural consideration in tool-path planning, this research presents a novel FDM method unifying structural performance considerations at the scale of global geometry, topology, and filament layout. Oriented material deposition

along 3D principal stress vectors is identified as the candidate for developing a structurally informed tool-path planning strategy that integrates both manufacturability and structural objectives, maximizing the structural strength-to-weight ratio for structural prints. In this regard, this research expands on existing works attempting similar approaches, most notably Chen *et al.*'s framework for subdividing planar surfaces to approximate Michell's optimal structure using stress line information.<sup>8,9</sup> The research presented in this study addresses limitation found in the early adaptation of the stress line method in AM, which includes a lack of consideration of the fabrication process and the material structure of FDM-produced parts, and the lack of physical results for comparative evaluation of printed geometries.

To motivate the research that is premised on the need to align structural behavior at the scale of geometry and material structure, this article began with an introduction of the problem of FDM-induced anisotropy in commercial platforms using experimental results. Fundamental structural mechanics principles that form the basis of the stress line-based techniques are then reviewed: Principal Stress Lines Derivation Review section, Stress Line Geometric Properties and Applicability in FDM section, System, Scope, and General Framework section, and Stress Line Generation Process section, respectively, summarize the theory of principle stress lines, identify the geometrical compatibility of stress line-based topologies to FDM processes, outline the general framework of SLAM, and describe the process for generating and adapting stress lines. Finally, this article provides results for the implementation of SLAM on two different platforms: methods and results analyzing the performance of printed parts produced with SLAM are shown in Implementation 1: SLAM for Planar Cases on Commercial Platform section for planar geometries using a commercial FDM platform, and in Implementation 2: Robot-Enabled SLAM for 2.5D Cases section for 2.5-D surfaces using an experimental robotic process.

#### Stress Line Theory and Applications

##### Principal stress lines derivation review

Principal stress lines are numerical integrations of principal stress directions over a design domain. Mohr's circles can be constructed to obtain the information required for constructing principle stress lines. Visually, stress lines indicate the directions of space where stress is purely axial. As a consequence, any elementary section (for 2D) or volume (for 3D) orientated along lines of principal stress will not be subjected to any shear (or bending) stress. Architectural and structural designers have routinely used stress lines to

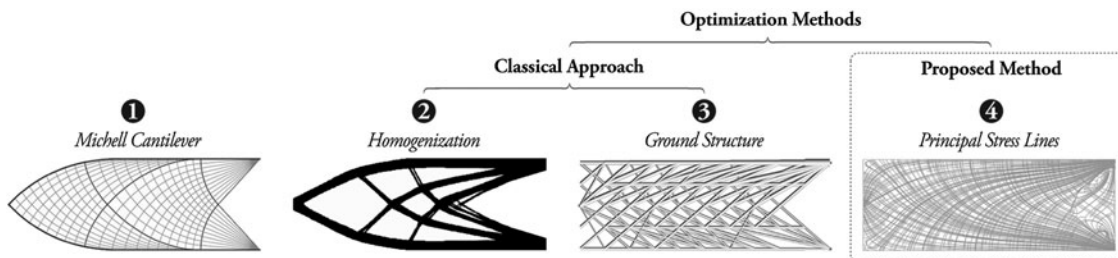


FIG. 5. Convergence of optimization results obtained from (2–3) classical optimization methods and both the (1) Michell structures and the (4) principal stress lines of the corresponding design domain.

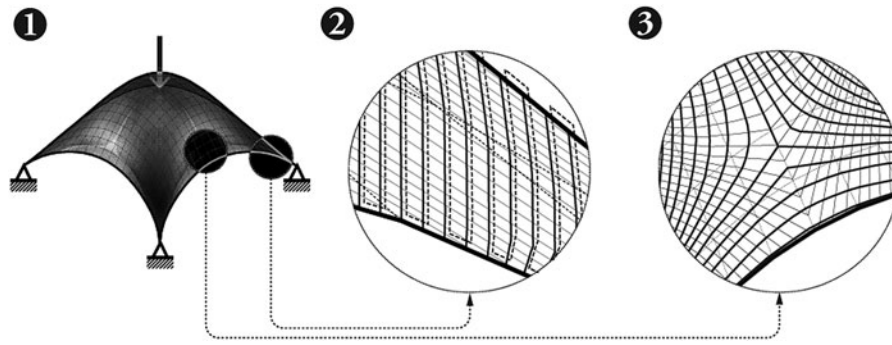


FIG. 6. General geometrical properties of stress line-based filament layout illustrated on a (1) funicular 4-support shell structure: (2) parallel-like curve geometries allowing efficient zigzag-like path linkages; and (3) geometrical similarities between stress lines and design boundaries.

visualize the natural force flow of an applied load through a structural system,<sup>28</sup> which approximately indicates the desirable material continuity for a given design domain.<sup>29</sup>

The study of stress lines is related to Michell's classical studies on structural optimization.<sup>30</sup> Michell's theory states that a framework  $S$  within a region of space  $R$  resisting a loading  $Q$  will be of minimal volume if (1) any of its members are stressed up to their maximal allowable compression or tension stress; and (2) members of  $S$  are subjected to the same strain  $\epsilon$  in absolute value, with  $\epsilon$  defined as the maximum allowable strain within  $R$ . As denoted by Chen,<sup>8</sup> Hemp,<sup>31</sup> or Strang and Kohn,<sup>32</sup> such conditions imply that the members of  $S$  will lie along the lines of principal strains within  $R$ . Since stress and strain have the same principal directions, as Hooke's law in linear elasticity for isotropic material indicates, the structures derived from principle stress line methods are related to the optimal structures theorized by Michell, providing an explanation to the design convergence that is typically evident between the results of classical optimization methods (Fig. 5.2, 5.3) and both the principal stress lines (Fig. 5.4) and the Michell structures (Fig. 5.1) of the corresponding design domain.<sup>33</sup>

#### *Stress line geometric properties and applicability in FDM*

While previous research has provided theoretical support for the use of principle stress lines to generate high-performing topologies that approximate optimal-like structures for the same boundary condition, this article has identified stress line properties that suggest significant compatibility with FDM-based operations:

**Geometrically compatible path planning.** Since stress distribution for elastic continuum bodies are also continuous, stress lines create contour-like and near-parallel fields of curvatures traversing from one design boundary to another, thereby producing geometric properties consistent with filament layouts generated by conventional FDM path filling techniques, such as CPP (Fig. 4.1) or DPP (Fig. 4.2) planning.<sup>34</sup>

In common with CPP, which uses successive offsets of the boundary curves as tool-paths, stress line-based filament layout encourages articulated and smooth finishing because stress lines are geometrically similar to the design boundary of printed parts in general, as Figure 6.3 shows. Similarly, the parallel-like geometry of stress line-based filament layout allows efficient zigzag-like path linkage with low jump distances (Fig. 6.2), thereby contributing to the fabrication efficiency commonly associated with DPP, which is characterized by the line-by-line filling of an area at a specified orientation.

**Computational ease.** As illustrated by Figure 7.2 and 7.3, conventional numerical optimization methods tend to produce complex results that are computationally expensive to solve and geometrically difficult to manipulate and adapt<sup>4</sup>; there is, in fact, no guarantee that the structure generated will be reasonable because numerical computation can become unstable when large number of design variables are present,<sup>35</sup> as is frequently required in complex designs. Conversely, stress line methods produce discrete curvatures that can readily be converted to tool-paths (Fig. 7.1). Computational ease of SLAM is also notable: existing path filling strategies rely on geometric operations that are more computationally complicated and expensive than the Finite Element Analysis (FEA) relied by the stress line method.

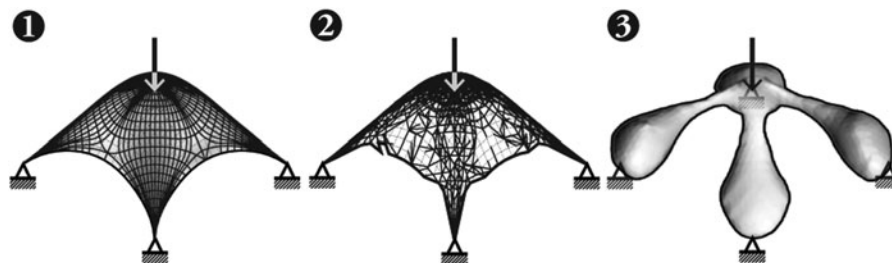


FIG. 7. Diagram showing the (1) adaptability of stress line results as printing tool-paths, in contrast to the geometrically complex and noisy results typically produced by classical optimization approaches using (2) ground structure and (3) homogenization method.

## Stress Line Additive Manufacturing

The proposed SLAM method is motivated by the objective to develop FDM as a high-performance fabrication method capable of producing specimens that accurately convey both geometry and the structural performance expected of the specimens' geometry and intended application, such that FDM can be reliably used to create mechanically meaningful pieces that can be comparatively tested at the prototyping scale, or end-use functional parts at full scale like building components. The workflow to implement SLAM consists of the following steps: (1) stress line computation, which encompasses initialization, generation, and adaptation of stress lines for AM; (2) digital fabrication, which includes structurally informed methods for converting stress line-based geometries into fabrication instructions; and (3) experimental load testing. Presented are two implementations of SLAM: using a commercial platform and a custom extrusion module attached to a robotic arm.

### *System, scope, and general framework*

The SLAM method works with FDM for several reasons: it is cost-effective, widely used by designers, and produces parts that are relatively strong and durable.<sup>36</sup> With fewer fabrication processing parameters of relevance compared to other AM processes, such as selective laser melting (SLM),<sup>37–39</sup> unexpected performance interactions due to fabrication idiosyncrasies are also minimized.

To maximize the design relevance of the proposed framework among architects and engineers, the research was developed using the popular 3D modeling tool Rhinoceros 3D,<sup>40</sup> within the parametric visual programming language environment of Grasshopper 3D.<sup>41</sup> Structural analyses were conducted using the FEA plug-in Karamba.<sup>42</sup> This research also utilizes Goat,<sup>43</sup> which is an optimization solver that relies on gradient-free optimization algorithms found in the NLOpt library.<sup>44</sup>

Geometrically, the implementation demonstrated in this article focuses on both planar and form-found 2.5D membrane structures. Since these systems are subjected only to in-plane stresses, normal stresses in discretized members are primarily axial-only with negligible bending, thereby creating a suitable design test case to validate the advantages of the proposed technique in addressing FDM-induced anisotropy.

**Stress line generation process.** Stress line construction methods are primarily numerical and iterative because analytical versions are often difficult to formulate. Consequently, the qualities and usability of stress lines vary widely according to the various construction and calculation parameters. The computation of stress lines in this research follows a methodology outlined in the author's previous work,<sup>45</sup> which was built on the foundational research conducted by Chen *et al.*,<sup>8,9</sup> and Michalatos and Kaijima.<sup>29</sup> The proposed approach addresses known problems in commercially available approaches, such as (1) low stress line resolution, (2) poor stress direction interpolation, and (3) stress line discontinuities.<sup>46</sup> Contrasting existing approaches focused on force visualization; the method developed by the authors seek to generate optimal-like frame topologies with proper connectivity that can be easily fabricated through AM.

The fundamental procedure has been broken into the three stages of initialization, generation, and processing.<sup>45</sup> The purpose of initialization is to characterize the design domain with proper meshing and conduct structural analysis on the design domain to obtain data needed for stress line construction. Following initialization is generation: given a seeding point, the principal stress directions are extracted from the underlying FEA data and interpolated for that point. A line segment is then drawn along these directions and its endpoint becomes the starting point for the subsequent iteration. This process repeats until the stress line reaches the design boundaries; the conclusion of the stress line for one seed leads to stress line construction for the next seed in the sequence.<sup>46</sup>

Obtaining a uniformly spaced base stress line field, structurally informed methods are used to process and select stress lines for AM since the theoretically optimized Michell-like optimum structure, which has an infinite number of infinitely small bars with infinitely low stress, is neither manufacturable nor significantly superior in structural performances than those at lower density.<sup>47</sup> Modifications have been introduced to the methods developed in previous research to consider the fabrication constraints that are particular to each implementation presented, encompassing both selection and correction methods.

To measure structural efficiency, this article uses the minimization of strain energy as the objective function, also referred to as the minimization of compliance, or the maximization of stiffness.<sup>48,49</sup> Performance comparison of stress line-based structures is enabled by normalizing strain energy with the total member length and by holding constant the total magnitude of external loads applied, loads that are then redistributed to each node according to its respective tributary area estimated using a Voronoi-based method.<sup>50</sup>

### **Implementation 1: SLAM for Planar Cases on Commercial Platform**

Developed in the first implementation is a method for enabling SLAM on existing commercial FDM platforms to create high-performance planar structures such as beams. The two-part investigation seeks to provide confirmation that structural performance is maximized when continuous material deposition is parallel to the primary plane of structural action and when in-plane filament layout is aligned to stress line-based topology.

### *Hardware setup, and design and planning of comparative structural load testing*

The specimens are produced in ABS plastic with a Stratasys Dimension sst 1200es 3D printer,<sup>51</sup> using the "Solid" interior density setting, which ensures tight filament packing to facilitate force transfer, and the "SMART" setting, which ensures support material is assigned to only the most critical locations. The fabrication of the specimen relies on the filament layout generated by CatalystEX,<sup>51</sup> which is the Stratasys software package for converting the CAD-generated Standard Tessellation Language (STL) output into the filament layout and printing instructions. Three identical prints and tests are conducted for each design case.

Figure 8 illustrates the standard naming convention adopted in this article to describe the element's orientation and parts. All test cases were designed and specified as



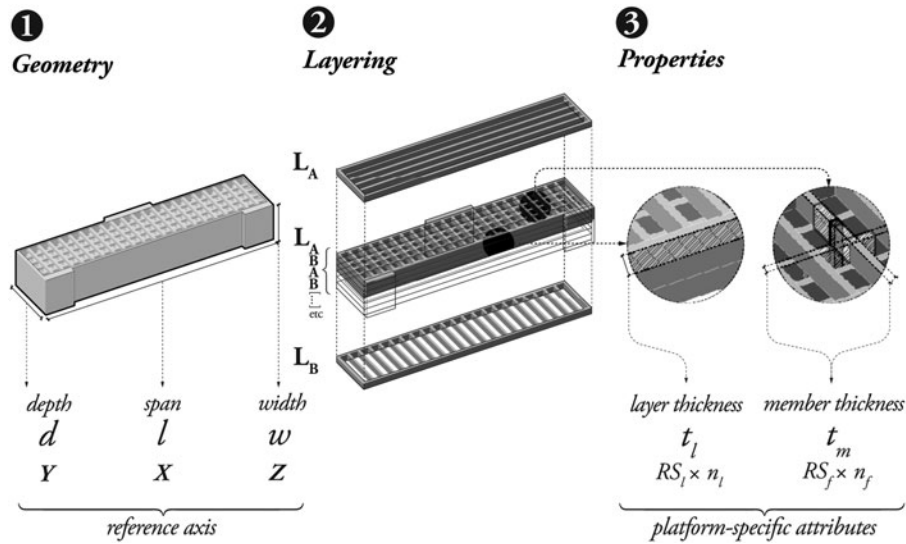


FIG. 8. Diagram showing the orientation, labeling terminologies, and geometric attributes of test cases at the scale of the (1) global geometry; the (2) alternating topology layers; and (3) the members within the layers.

simply supported beam trusses with load applied at mid-spans, providing a complex and realistic comparative structural configuration for understanding the effects of anisotropy and topology (Fig. 8.1). The span of the structure is the maximum printable span achievable with the print bed of the Dimension, which is 150 mm. To prevent out-of-plane buckling, all trusses are provided with 30.5 mm in width. All test designs are encased within a rectangular enclosure. A platform is provided both at the area of supports and load application for force distribution (Fig. 8.2).

Strategies for member and filament orientation alignment. In cases where print layers are parallel to the plane of structural action, two general fabrication-driven geometrical design strategies were devised to ensure parallel alignment of the filament and the internal members of the beam trusses. The first strategy sets the thickness of the internal members as integer multiples of the filament resolution (Fig. 8.3) to encourage the default CatalystEX path filling algorithm to achieve filament member alignment by creating paths through simple offsetting of internal members. The second strategy involves the reduction of in-plane member intersections as the default algorithm generates unaligned filament layouts in areas near members' intersections.

Organizationally, since all design cases include two distinct classes of members, in-plane intersections can be mitigated by modeling the beam trusses as stackings of two alternating topology layers (Fig. 8.2). This article also proposes a two-step processing method for generating stress line-based designs, which incorporate Dimensions' fabrication constraints, from an initial base dense stress line field. The first step begins with the selection of a starting stress line, followed by the incremental evaluation of adjacent stress lines for their maximum point-to-point distance with the selected starting stress line. The first stress line that fulfills the maximum spacing target (See Row PR1 in Fig. 9), which is user defined according to material quantity and aesthetic constraints, and is measured according to the maximum point-to-point distance between adjacent stress lines is selected. The iterative search process then repeats again for the

newly selected line. With all stress lines in the base stress line field evaluated, the second iterative procedure then removes, according to a target minimum point-to-point distance, the remaining stress lines that are causing in-plane intersections (see row PR2 in Fig. 9). In ensuring that the selection of stress lines will fulfill basic maximum and minimum spacing criterion, the outlined approach provides indirect mechanisms for affecting the density of the stress line-based system. However, because of variations in the resolution of the base dense stress line field and discrepancies between the overall spacing of adjacent stress lines and their maximum point-to-point

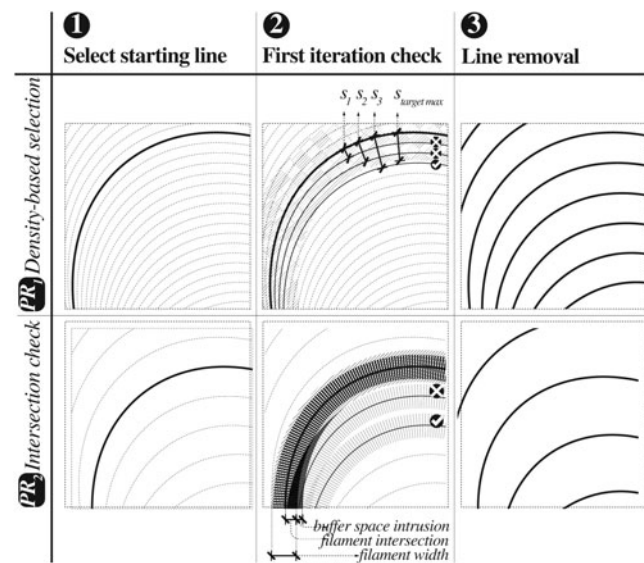



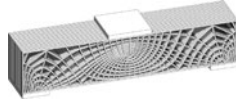
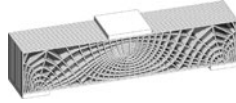
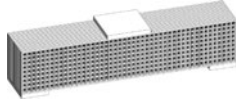


FIG. 9. Rule-based corrections for adapting SLAM to commercial FDM platforms. The figure illustrates the first three steps applied for each rule (PR1-2), which consists of (1) selection of starting line; (2) stress line evaluation and selection for inclusion (✓) or removal (×); and (3) line removal. FDM, fused deposition modeling; SLAM, Stress Line Additive Manufacturing.

TABLE 2. DIGITAL MODELING AND DESIGN OF TEST SPECIMENS USED IN INVESTIGATION ONE

Case	SLAM-XY	SLAM-XZ	Grid-XY
Member Center lines			
Fabrication instructions in Standard Tessellation Language (STL) geometry			
Bounding box dimensions Volume V (mm <sup>3</sup> )	151.9×37.6×30.5 mm (6.0×1.5×1.2 in) 35,260		

SLAM, Stress Line Additive Manufacturing.

distances, this indirect strategy cannot guarantee consistent and uniform spacing in the produced stress line-based designs. Future implementation will develop computational selection methods based directly on overall density considerations.

**Test cases designs.** As described in Table 2, the first investigation fabricates an identical stress line-based geometry at two print orientations. SLAM-XY, which serves as the control case for both investigations, has layers that are parallel to the plane of structural action formed by the depth and span of the beam truss and a filament layout that generally maintains parallel filament member alignment, thereby enabling the effective utilization of the material yield strength. Conversely, in SLAM-XZ, internal members are constructed through layer-by-layer material deposition, such that the structural performance of the beam truss is controlled by its layers' fusion strength.

To test the effects of topology on structural performance, the second investigation implements an alternative 2D Vierendeel-like grid frame topology (GRID-XY), which is characterized by beam truss discretization as frames with

rectangular and untriangulated openings, as Table 2 illustrates. An attempt was made to calibrate the member width and density to equalize the volume and weight of all design cases. Three identical specimens were produced from each of the three cases, resulting in nine tested specimens.

*Documentation, analysis and discussion of results*

Table 3 includes the fabrication instruction generated for the Dimension printer, and Table 4 provides quantitative and photographic documentation of all fabricated results. As expected, the finishing quality is superior in test cases that are printed parallel to the plane of the beam truss topology, as demonstrated in the comparison of SLAM-XY and SLAM-XZ in Table 4. In the latter case, an undulating variation in cross-sectional diameter along the internal members' length is noticeable due to the length-wise layer-based material deposition. Discrepancies in mass have also been observed despite the use of identical print settings, and the equalization of volume for all cases, the difference, which is quantified by the mass-to-volume ratio, or density, suggests inconsistency

TABLE 3. DOCUMENTATION OF FABRICATION SETUP AND INSTRUCTIONS

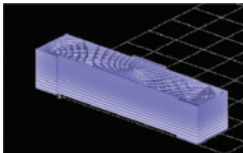
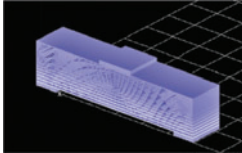
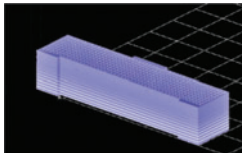
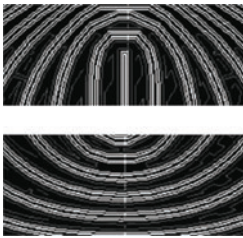

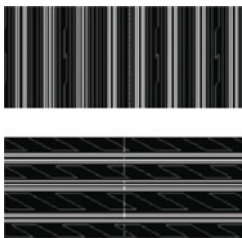
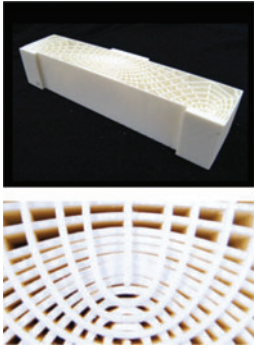
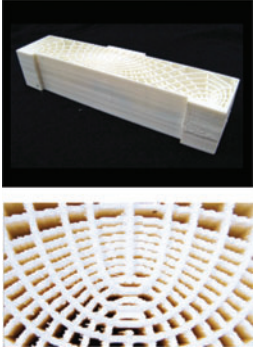
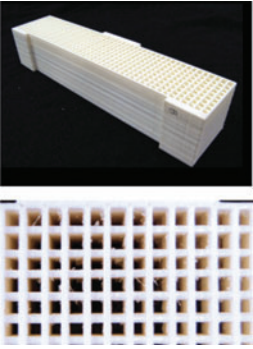
Case	SLAM-XY	SLAM-XZ	GRID-XY
Print model space setup			
Layer pattern or filament layout			
Fabrication time	9 h: 11 min	143 h: 35 min	19 h: 08 min
Model and support material requirement (mm <sup>3</sup> )	55,060.5; 64,565.0	46,867.0; 67,842.4	58,378.0; 67,187.0

TABLE 4. DOCUMENTATION OF FABRICATED TEST SPECIMEN

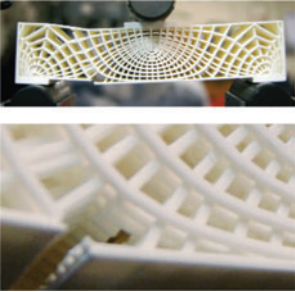
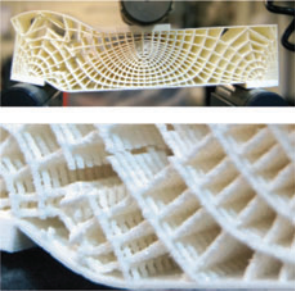
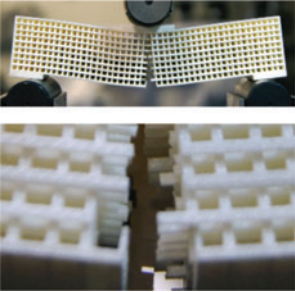
Case	SLAM-XY	SLAM-XZ	Grid-XY
Fabricated results Overall view Detailed elevation view			
Mass, $m$ (g)	46.5	54.2	62.6
Density, $D = m/V$ ( $\text{kg/m}^3$ )	1317.6	1536.3	1726.0

in the packing intensity of the filament material by the Dimension platform. All results are normalized according to the specimen mass to account for these discrepancies.

Load testing and load-displacement plot results of the comparative load testing for both investigations are respectively summarized in Table 5 and Figures 10 and 11. As Table 5 shows, the normalized ultimate and yield load-to-weight ratios for SLAM-XY are respectively 3.5 and 4.7 times higher than SLAM-XZ's ratios. In addition, SLAM-XZ behaves with

considerably more ductility (Fig. 10), with yield capacity sustained through extensive plastic deformation. The significant performance difference indicates that the print orientation has a critical impact on structural behavior, thereby reaffirming the problem of anisotropy in specimen printed using layer-based processes. Support for this interpretation is also evident in the specimens' failure mode, whereas SLAM-XY experienced simultaneous gross section tensile failure along the member where the greatest tensile stress is expected; the failures of

TABLE 5. DOCUMENTATION OF FAILURE MODES AND COMPARISON OF PREDICTED AND ACTUAL LOAD TESTING RESULTS NORMALIZED ACCORDING TO THE SPECIMEN MASS

Case	SLAM-XY	SLAM-XZ	Grid-XY
Predicted normalized yield load and displacement	2495.1 N/N at 0.79 mm		2250.1 N/N at 5.12 mm
Average normalized yield load and displacement	2537.7 N/N at 2.26 mm	541.6 N/N at 0.64 mm	1783.0 N/N at 2.93 mm
Average normalized ultimate load and displacement	2847.8 N/N at 2.92 mm	810.9 N/N at 2.46 mm	2799.9 N/N at 7.54 mm
Average elastic stiffness normalized by specimen mass	1111.8 (N/N)/mm	836.4 (N/N)/mm	601.6 (N/N)/mm
Failure mode description	Simultaneous gross section failures (tension) at concentrated location	Delamination between layers (tension) along Y axis, progressive failure at multiple locations	Gross section (tension), multiple locations
Failure type	Brittle	Ductile	Brittle
Failure profiles Global geometry Member view			

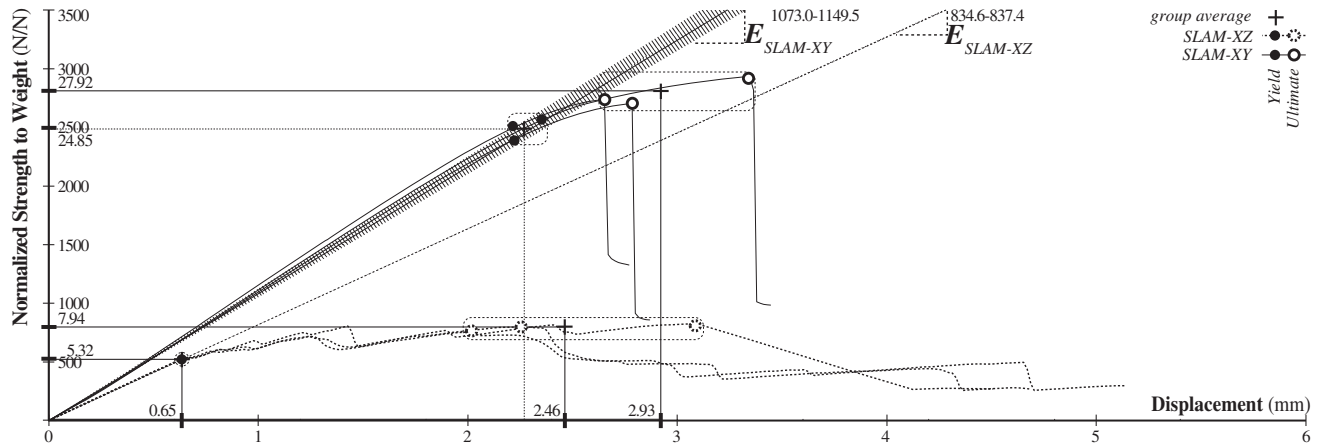


FIG. 10. Load-displacement plot for investigation one's test cases.

SLAM-XZ are progressive and numerous, characterized by delamination of the layers composing the length of internal members. The results of the second investigation are consistent with the initial prediction that stress line-based topologies are stronger than grid-based topologies (Fig. 11). Although the difference in ultimate load-to-weight ratio is subtle, with only an 8% difference between SLAM-XY and GRID-XY, a clear gain in yield strength is noticeable for SLAM-XY, as its yield load-to-weight ratio is 1.6 times GRID-XY's ratio. Figure 11 further shows higher stiffness for SLAM-XY through the load-displacement slope, which is 1.9 times steeper compared with GRID-XY. This indicates that the stress line-based structures exhibit truss-like behavior, whereas the grid-based structure behaves mostly in bending, which consequently uses the material less efficiently.

With an average normalized yield strength capacity of 2537.7 N/N, the experimental result for SLAM-XY is consistent with an FEA prediction of 2495.1 N/N (linear elastic assumption, yield is considered to occur when the first member fails). This closeness in yield capacity contrasts with the discrepancy observed for the GRID-XY specimen, where an 18% difference in yield capacity is noticeable. Two factors may explain the difference in performance for the GRID-XY specimen. First, geometric discrepancies have been identified

between the digital and fabricated model, discrepancies caused by idiosyncrasies of the default printer software used to convert the CAD-generated STL output into the filament layout and printing instructions. Measurements show that the horizontal members of GRID-XY were printed with reduced depth. Second, the numerical prediction relies on idealized structural assumptions, such as the in-plane coincidence of members' center lines at the joint intersections and the characterization of joints as fixed connections. These assumptions do not account, respectively, for the eccentricities introduced by the stacking strategy of alternating topology layers and the weakening of the joint connection as a result of structural action needing to transverse the weak bonds between the alternating layers. Consequently, GRID-XY has underperformed by 20.8% in comparison to its expected performance predicted using FEA; since the structural action of the topology is bending dominated, the reduced capacity of the joints would likely have a greater impact than is the case for SLAM-XY, which is predominantly governed by axial forces.

Regardless of the discrepancies identified above, it is clear from both investigations that filament alignment plays an important role in determining the structural performance of AM-produced parts. Significantly, there is validation that the SLAM method achieves parts with higher strength and

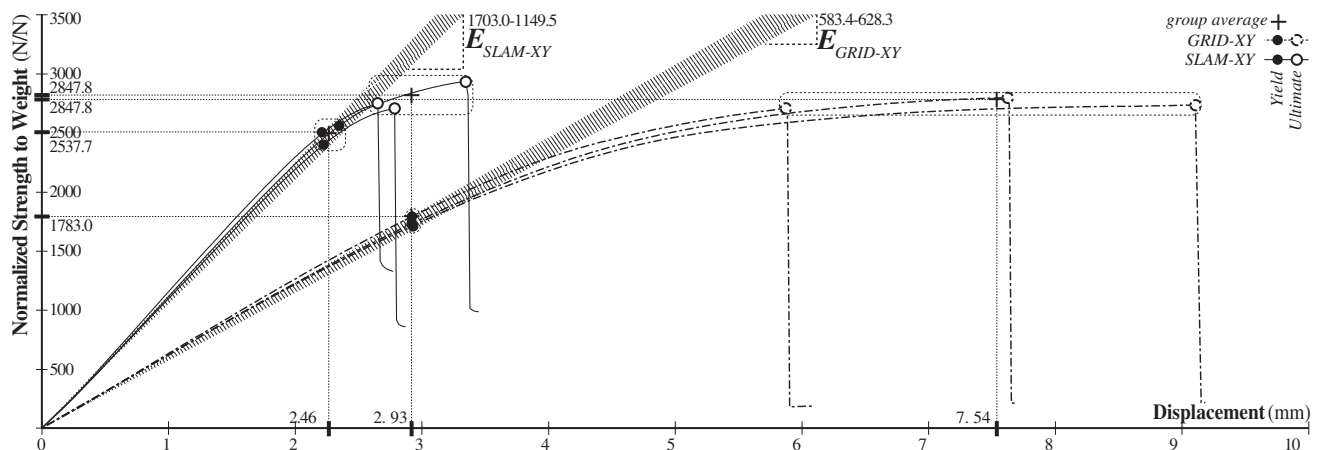


FIG. 11. Load-displacement plot for investigation two's test cases.



FIG. 12. Robotic fabrication work-cell setup. Photographic documentation of the robotic-enabled stress line additive manufacturing process: (1) robotic work cell; (2) oriented filament deposition of stress lines on substrate built from medium-density fiberboard; and (3) close-up detail of extruded filament.

stiffness. However, the encouraging results seen in the planar implementation will not be reproducible for highly complex 3D geometries, because their structural behavior cannot be reduced to a single planar orientation to be parallel with the print bed. This means that conventional monolithic printing methods, which are configured to be

able to achieve only continuous filament deposition in two directions, will produce 3D geometries that are affected by anisotropy, and therefore cannot be used to manufacture 3D structurally isotropic prototypes, or end-use parts that accurately model the structural behavior of the final geometry.

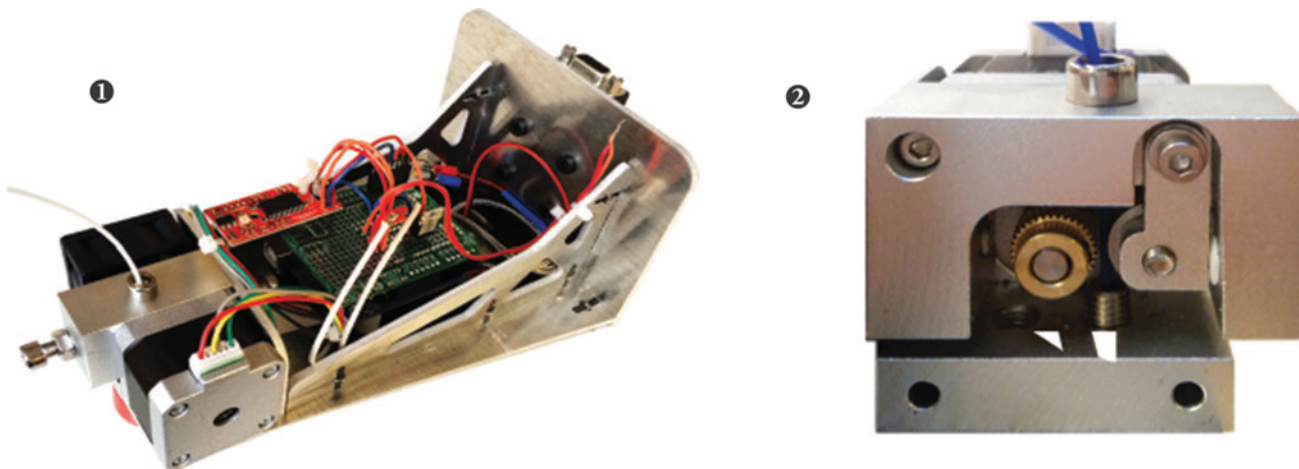


FIG. 13. Components of custom FDM printing module. (1) Custom FDM printing module; and (2) extruder head powered by Signstek stepper motor.

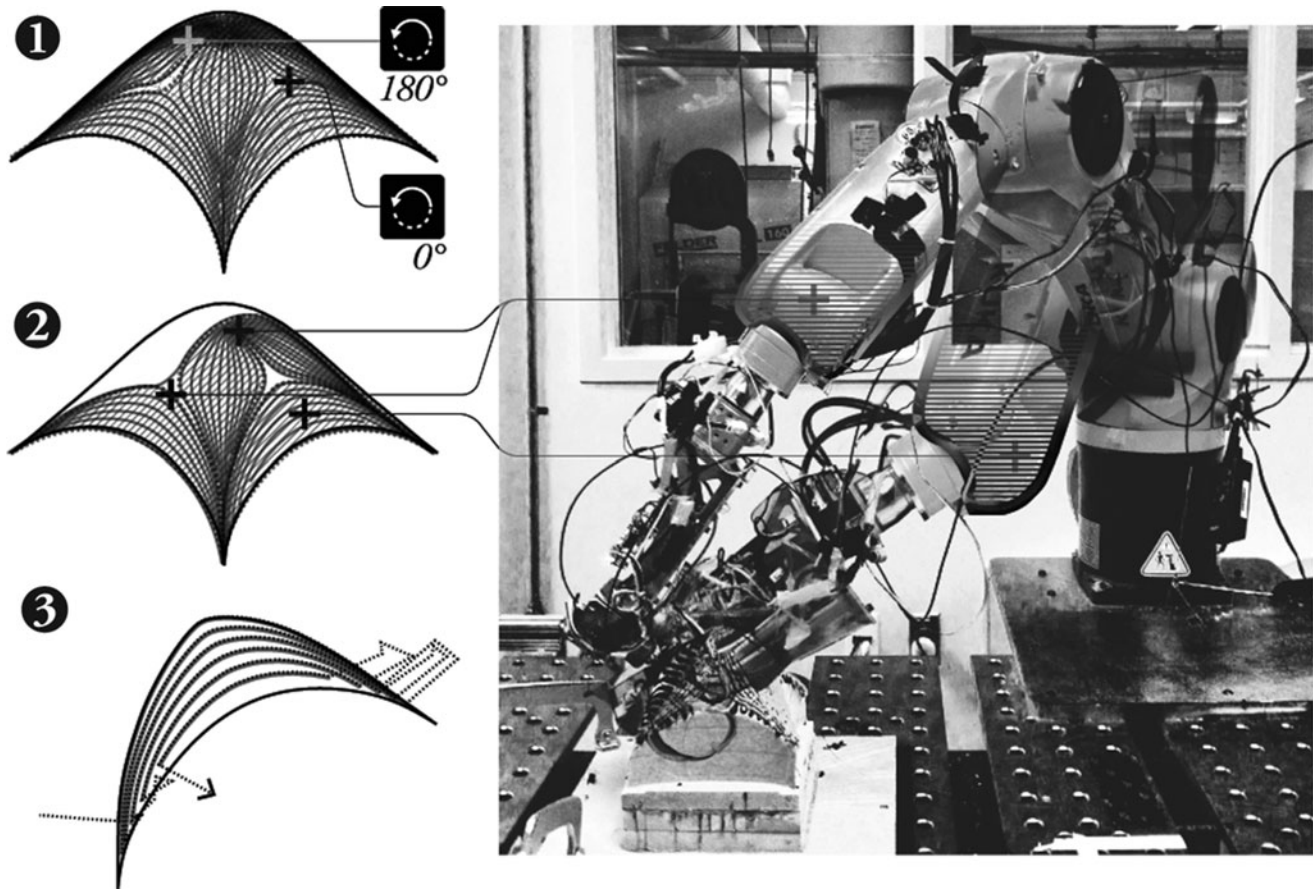


FIG. 14. Diagram showing the clustering of stress line-based paths into individual tool-path chains (2–3), based on the (1) positioning of the substrate; and (2) geometrical similarities of the individual paths.

### Implementation 2: Robot-Enabled SLAM for 2.5-D Cases

#### Problem and objective

The current challenges of AM techniques in aligning filament deposition to the directions of structural action for complex 3D design are due to the limited capacity of a conventional layer-based extruder to achieve varied orientations. In response, this article proposes a new adaptation of SLAM that combines stress line-based computation with multiaxis robot machining. The proposed method aims to allow for oriented filament deposition along the networks of axial structural actions on complexly curved surfaces.

#### Software and hardware framework

This second implementation uses the KUKA KR6 R900 sixx small robot,<sup>52</sup> which is mounted with a custom extrusion module, and is centrally located inside a contained work cell. As shown in Figure 12.1, the medium-density fiberboard (MDF) surface printing bed is clamped to the metal work table at an eccentricity from the robot to minimize robotic joint rotational issues.

**Custom FDM printing module.** Based on research into consumer-grade extrusion devices, the custom extruder is composed of a waterjet-cut aluminum frame that is me-

chanically coupled to the robot by a pneumatic tool changer. The aluminum frame (Fig. 13.1) holds a commercially available extruder sold by Signstek<sup>53</sup> and control electronics (Fig. 13.2). The Signstek extruder accepts 1.75 mm PLA and is composed of a 1.8° stepper motor, heating element, thermistor, and cooling fan. Using an Arduino Uno<sup>54</sup> microcontroller and an N Type MOSFET, the closed loop temperature control of the extruder nozzle was utilized. The KUKA's 24 V signal outputs were monitored by the on-board Arduino and were used to start and stop the stepper motor/extrusion. Control of the stepper motor was achieved with an EasyDriver<sup>55</sup> board that uses an Allegro A3967 motor driver chip.

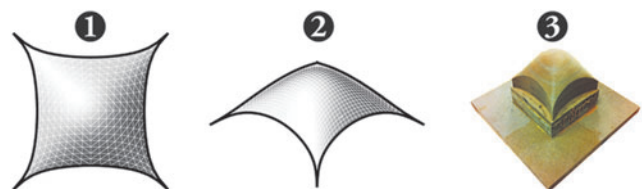


FIG. 15. Surface geometry used in implementation 2. Uniformly loaded four-support grid shell geometry used in implementation 2: (1) plan; and (2) axonometric view; and (3) printing substrate.

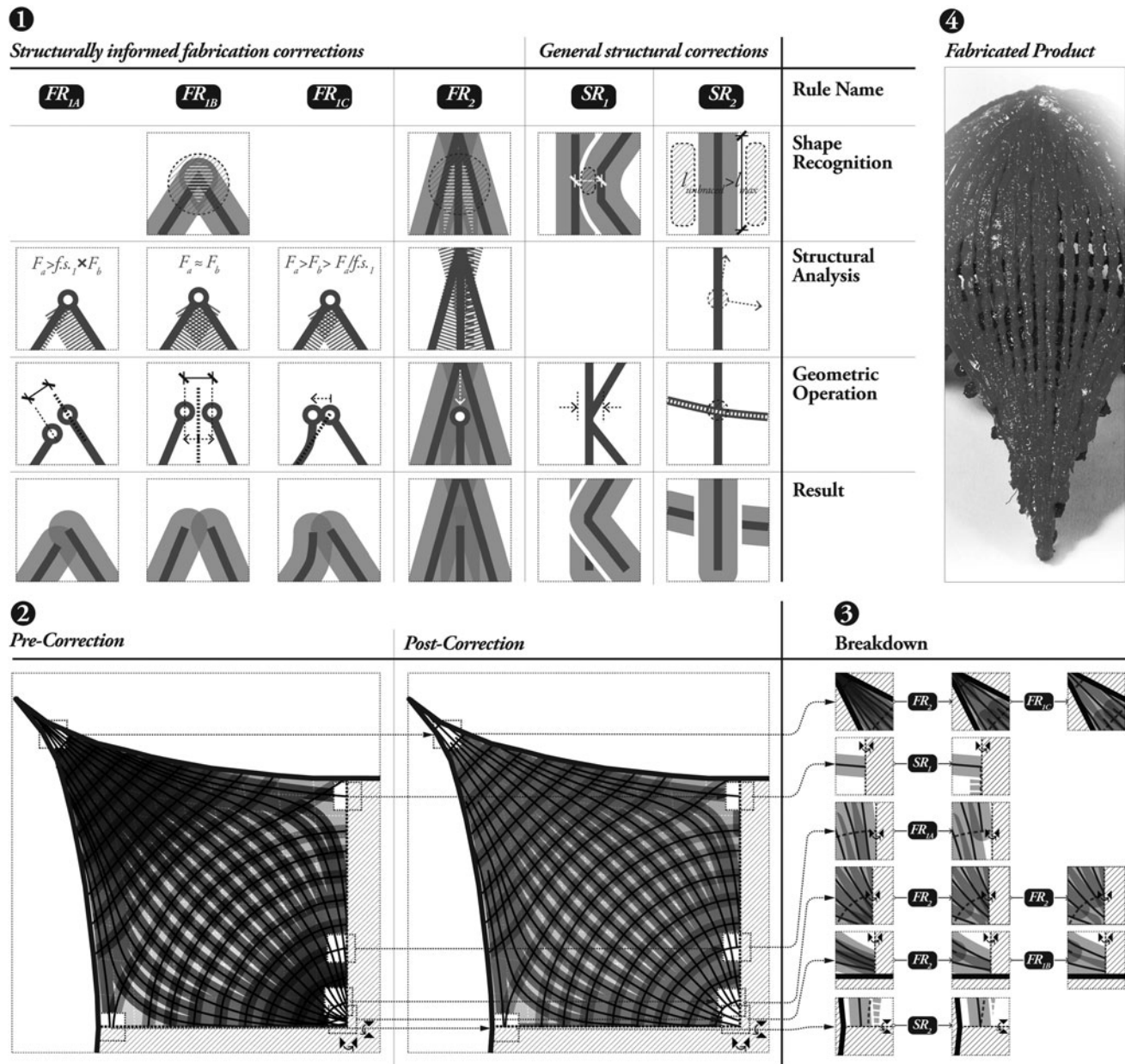


FIG. 16. Rule-based system developed to correct fabrication paths: (1) specific correction rules addressing fabrication or structural concerns; (2–3) application of various correction rules on the bisymmetrical region of a four-support grid shell design case; and (4) photograph of the fabricated specimen.

Robotic programming. The KUKA KR6 Robot arm is programmed with KRL code, and the robot instructions are generated in RobotMaster,<sup>56</sup> which is a plugin to MasterCAM.<sup>57</sup> The typical workflow consists of the following iterative and trial and error procedure: (1) import of print surface and stress line data from CAD into CAM software; (2) specimen positioning in the workspace; (3) print surface calibration in the CAM model space; (4) clustering of paths based on robot work volume and reach limitations trajectory (Fig. 14); (5) assigning stress line-based geometry for tool-path generation; (6) iteration of possible joint configurations in CAM and RobotMaster interface; (7) optimization and simulation of robot; and (8) export KRL code and run program in KUKA.

*Design and planning of comparative structural load testing*

The research of robot-enabled SLAM focuses on 2.5-D surface structures: the Kangaroo<sup>58</sup> plug-in was used to form-find a uniformly loaded basic grid shell with four supports, as demonstrated in Figure 15.1–15.3, the form-found printing substrate milled from a wood block consisted of laminated MDF layers.

Adaptation for robot-enabled fabrication. As in the approach taken in the first implementation, a series of rule-based corrections are specifically designed for the robot-enabled

TABLE 6. DOCUMENTATION OF 2.5-D FABRICATED TEST SPECIMEN

Case	MB-CT	MB-UDL	SL-DL	SL-PL	SL-ADL	SL-LL
Description	Constant surface thickness	Uniformly distributed vertical load		Central vertical point load	Asymmetrically distributed vertical load	Asymmetrically distributed horizontal load
Domain specification						
Principle stress line results						
Postprocessed stress line-based member Center lines	n/a					
Layer-1 Layer-2						
Fabrication instructions						
*Standard Tessellation Language (STL) geometry						
**Clustering of stress line-based paths						
Manufacturing Method	MakerBot Replicator 2 Horizontally layered deposition		Robot-enabled SLAM Oriented material deposition for member filament alignment			
Fabricated result						
Overall view Detail						
Copies tested	2	1	2	2	0	0

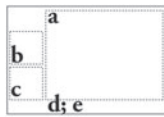
ADL, asymmetrically distributed load; CT, constant thickness; LL, lateral load; PL, point load.

extrusion platform, and iteratively applied to the initially obtained evenly spaced stress line field to achieve additional improvements in fabrication ease and quality (Fig. 16.2, 16.3). These include the removal of line segments in areas with significant stress line overlap, or the realignment of otherwise converging stress lines in highly stressed areas (Fig. 16.1, FR#). General structural rules include modification of stress line curvatures to facilitate force transfers at intersection nodes and the insertion of bracing members (Fig. 16.1, SR#). Although the initial implementation of the rule-based system

required some manual operations, the process can be automated in future developments.

Design of test cases. To validate that SLAM-produced specimens perform better than conventionally 3D-printed parts, a comparative load test was completed on a number of specimens: four printed using the SLAM method and three printed using a conventional layer-based 3D printer. MakerBot Replicator 2<sup>59</sup> was selected as the technology to be compared to the SLAM method, as it is





a: axonometric view  
b: plan: top view  
c: plan: under view  
d: specimen name  
e: load case

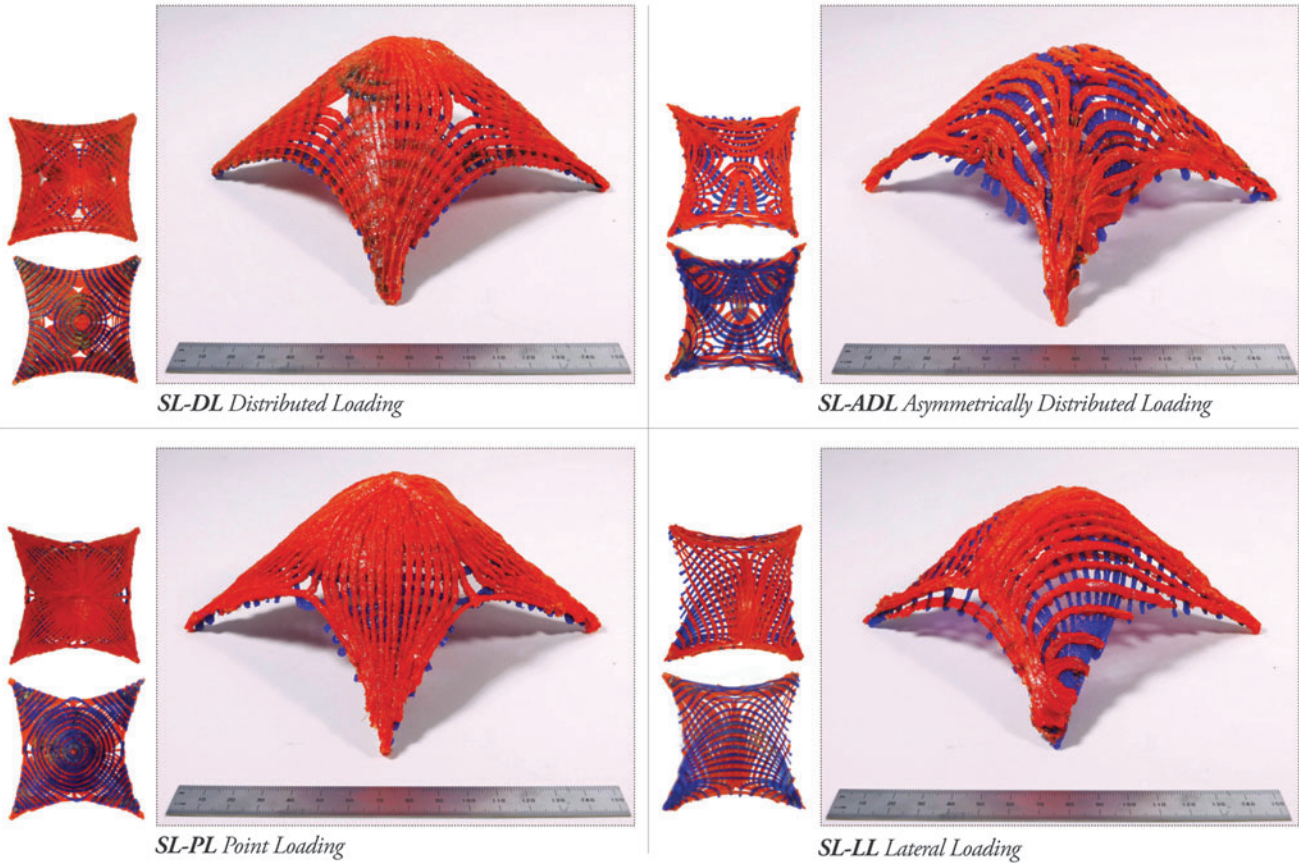


FIG. 17. Detailed photographic documentation of SLAM specimen.

one of the most popular consumer-grade 3D printing platform available to designers using PLA plastic. An effort was made to ensure that all specimens have similar total material volume. Table 6 describes the design and fabrication of the small-scale specimens for the four-support shell structure.

For the SLAM specimen, four loading cases were used to generate stress line-based topologies: (1) distributed load (labeled SL-DL); (2) point load (SL-PL); (3) asymmetrically distributed load (SL-ADL); and (4) lateral load (SL-LL). The resulting specimens produced from these load cases are shown in Figure 17. The MakerBot MB prints

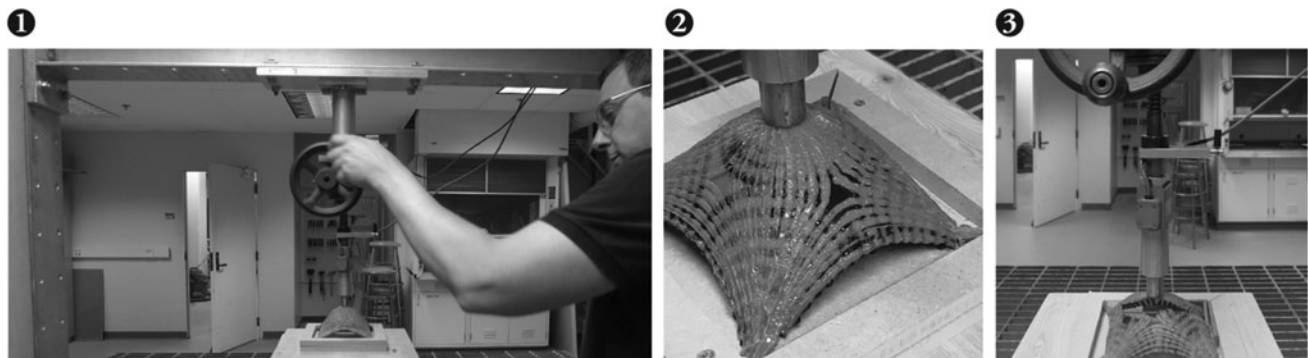
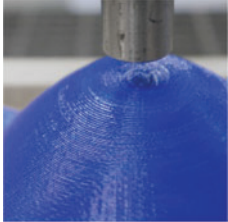
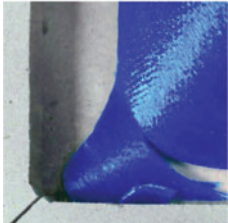
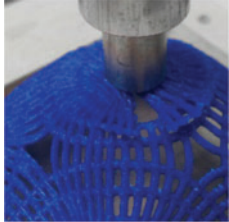
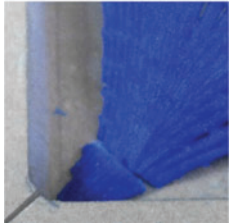
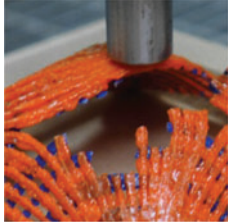
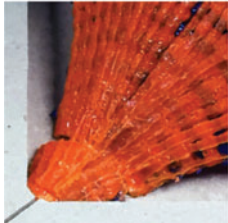




FIG. 18. Load testing setup. (1) Structural load testing setup showing (2) loading application and the (3) failure profile of a SLAM-produced specimen.

TABLE 7. DOCUMENTATION OF FAILURE MODES AND COMPARISON OF PREDICTED AND ACTUAL LOAD TESTING RESULTS NORMALIZED ACCORDING TO THE SPECIMEN MASS

<i>Specimen name</i>	<i>MB-CT</i>	<i>MB-UD</i>	<i>SL-DL</i>	<i>SL-PL</i>
Mass (g)	39.8	37.2	40.7	49.9
Normalized predicted initial yield load	1890.5 N/N	2411.2 N/N		3038.3 N/N
Normalized initial yield load	1685.1 N/N	1547 N/N	1817.5 N/N	1609.1 N/N
Normalized ultimate load	2045 N/N	2756 N/N	3603 N/N	2896 N/N
Peak elastic stiffness normalized by specimen mass	449.9 (N/N)/mm	647.3 (N/N)/mm	822.2 (N/N)/mm	736.8 (N/N)/mm
Failure mode description	Intralayer bond	Filament crushing, local fracture, intralayer bond	Filament crushing/bending, global fracture	Filament crushing/bending
Failure type	Brittle	Brittle	Ductile	Ductile
Failure profiles Top Corner	 	 	 	 

UD, distributed load.

included both a solid constant-thickness shell (labeled MB-CT) and a stress line-based topology based on SL-DL.

### Results

The load test consists of a single centralized vertical point load that was applied until a peak load was reached (Fig. 18); Table 7 shows the load testing results for the four cases with symmetrical vertical loading (MB-CT, MB-UD, SL-DL, and SL-PL). While the number of tests conducted is not high enough to be statistically conclusive, the preliminary results nevertheless suggest that the robot-enabled SLAM method can also lead to improved structural behavior compared to parts produced using commercial FDM platforms. Both numerical and experimental results demonstrate the benefit of material redistribution by stress lines, as seen in the improved strength performance of MB-UD over MB-CT. Similarly, the combined benefits of topology and filament-member alignment, which eliminate the problem of anisotropic behavior, are demonstrated by the improved performance

of SL-DL over both MB cases. The experimental results show that the SLAM cases registered a 25% improvement in stiffness, and a 76% and 27% improvement, respectively, in ultimate strength capacity and ductility after initial failure. The potential gain is particularly prominent in comparison to MB-CT, where intralayer bond failures occurred in areas where tensile stresses were predicted to occur (see “Failure profiles: Corner” in Table 7). More significant advantages for the SLAM method are expected in complex geometries and loadings that induce more tension.

Although the initial robot-enabled implementation is able to demonstrate the strength and ductility advantages achievable using SLAM for 2.5-D design cases, the comparison of the experimental and numerical results nonetheless show that all physically produced specimens have underperformed with regard to their initial yield capacities. For the MB specimen, the lowered experimental yield strength is expected because the layer-based extrusion of the conventional platform creates an anisotropic specimen with

reduced strength capacity, such that the ultimate yield strength for the MB specimen has barely exceeded their expected yield capacity (a paltry margin of 8–12% is observed). Conversely, the underperformance in yield strength for the SLAM specimen is largely the result of the fabrication technique's inconsistent quality control, inconsistencies such as fluctuating filament thickness, and width that may have led to premature initial failure of the specimen. This interpretation is supported by the capacity for all SLAM specimens to achieve some additional 80–100% increase in strength capacity following their initial failures, despite their underperforming initial yield loads. Additional evidences are found in the photographic documentation of SL-PL, whereby an unanticipated acceleration in printing speed due to robotic constraints has led to a narrowing of the filament extrusion near the corners where significant load paths converged (see "Failure: profiles: Corner for SL-PL" in Table 7), resulting in substantial discrepancy between the predicted and actual yield loads of SL-PL. It is clear that significant improvements to the fabrication technique are still needed; future improvements will allow the SLAM-produced specimens to better realize the potential strength and stiffness gain associated with stress line-based tool-path planning.

## Conclusion

### *Summary of contributions*

The research pursued in this article presents and validates a new approach to AM that synthesizes the design and optimization of FDM-produced part, where unlike conventional approaches, structural behavior of the printed parts is simultaneously considered at the scale of the geometry, topology, and filament layout. Structural load testing of two implementations provided initial verification that the proposed method outperforms methods using the conventional layer-based paradigm

### *Future work*

The success of the second implementation in achieving complexly curved 3D designs suggests that the greatest potential of the SLAM technique is to be gained by expanding the robot-enabled methods. In that area, there are several important directions for future development: (1) extensive experimental testing that incorporate the variations of both topology generation and fabrication parameter to better understand the material and strength behavior of SLAM-produced specimens; (2) standardization and improvement of the SLAM methods to achieve better precision and surface quality; (3) improved computational automation for integrating the stress line and robotic path generation and computational framework to automate the generating stress line-based structures and robot paths; and (4) expansion of the design applications of SLAM to enable the fabrication of printed parts with greater diversity of geometries and functionalities. Specifically, modification on the design boundaries and loading and support conditions of the design can produce test cases that offer a better understanding on the expected tensile strength improvement of SLAM-produced parts. Significant future milestones also

include the development of computational techniques for volume-filling 3D solids, such as by ongoing research to extend Michell's theory for 3D structural applications,<sup>60</sup> the elimination of the requirement of a printing support,<sup>61</sup> and the expansion of the extrusion module's hardware capabilities, such as the incorporation of sensors to allow extrusion parameters to vary intelligently according to emergent conditions of the as-built specimen. These advances will open possibilities for free-form and real-time AM, thus allowing the technique to be implemented for more complexly curve 3D surface design and full-scale construction.

## Acknowledgments

The authors wish to thank the following students who assisted with various aspects of this research: Jonathan Mackaman, Akshat Bubna, Elizabeth Bianchini, Nicholas Fine, James Coleman, Katie Gertz, Colin Poler, Xinyi Ma, Mitchell Gu, Chrystal Chern, Benjamin Jacot, and Yijiang Huang. Also, the authors acknowledge MIT fabrication laboratory coordinators Justin Lavalley, Chris Dewart, Jen O'Brien, shop monitors Inés Ariza, and James Addison, and testing laboratory technician Stephen Rudolph.

## Author Disclosure Statement

No competing financial interests exist.

## References

- Christensen C. The ongoing process of building a theory of disruption. *JPIM* 2006;23:39–55.
- Hopkinson N, Hague R, Dickens P, eds. *Rapid manufacturing: An industrial revolution for the digital age*. Chichester, England: John Wiley & Sons, 2006.
- Schmidt G, Druhl C. When is a disruptive innovation disruptive? *JPIM* 2008;25:347–369.
- Brackett D, Ashcroft I, Hague R. Topology optimization for additive manufacturing. *Proceedings of the Freeform Fabrication (SFF) Symposium*. Austin, TX: SFF, 2011; pp.348–362.
- Brandt M, Sun S, Leary M, *et al.* High-value SLM Aerospace components: From design to manufacture. *Adv Mater Res* 2013;633:135–147.
- Cooper DE, Stanford M, Kibble KA, *et al.* Additive manufacturing for product improvement at Red Bull Technology. *Mater Des* 2012;41:226–230.
- Ventola CL. Medical applications for 3D printing: Current and projected uses. *PT* 2014;39:704–711.
- Chen Y, Li Y. Beam Structure Optimization for additive manufacturing based on principal stress lines. *Proceedings of the 21st Solid Freeform Fabrication (SFF) Symposium*. Austin, TX: SFF, 2011; pp.666–678.
- Chen Y, Kwok T-H, Li Y. A structural topology design method based on principal stress line. *Comput Aided Des* 2016;80:19–31.
- Mueller CT, Irani A, Jenett BE. Additive manufacturing of structural prototypes for conceptual design. *Proceedings of the 55th International Association of Shell and Spatial Structures (IASS) Symposium: Shells, Membranes and Spatial Structures*. Brasilia, BRA: IASS, 2014.
- Bagsik A, Schoepner V, Klemp E. FDM part quality manufactured with Ultem\*9085. *14th International Scientific*

- Conference on Polymeric Materials, 2010, Halle (Saale), Germany.
12. Rodríguez JF, Thomas JP, Renaud JE. Mechanical behavior of acrylonitrile butadiene styrene (ABS) fused deposition materials. Experimental investigation. *Rapid Prototyping J* 2001;7:148–158.
  13. Ahn SH, Montero M, Odell D, *et al.* Anisotropic material properties of fused deposition modelling ABS. *Rapid Prototyping J* 2002;8:248–257.
  14. Ziemian C, Sharma M, Ziemian S. Anisotropic mechanical properties of ABS parts fabricated by fused deposition modelling. In: Gokcek M (Ed). *Mechanical Engineering*. InTech, Rijeka, HRV, 2012; pp.59–180.
  15. D'Amico A, Debaie A, Peterson AM. Effect of layer thickness on irreversible thermal expansion and interlayer strength in fused deposition modeling. *Rapid Prototyping J* 2017;5:23.
  16. Mueller J, Shea K, Daraio C. Mechanical properties of parts fabricated with inkjet 3D printing through efficient experimental design. *Mater Des* 2015;85:902–912.
  17. Keszy A, Kotlinski J. Mechanical properties of parts produced by using polymer jetting technology. *Arch Civ Mech Eng* 2010;3:37–50.
  18. Zhu Y, Tian X, Li J, *et al.* The anisotropy of laser melting deposition additive manufacturing Ti–6.5Al–3.5Mo–1.5Zr–0.3Si titanium alloy. *Mater Des* 2015;67:538–542.
  19. Frazier WEJ. Metal additive manufacturing: A review. *J Mater Eng Perform* 2014;23:1917–1928.
  20. Sun Q, Rizvi GM, Bellehumeur CT, *et al.* Effect of processing conditions on the bonding quality of FDM polymer filaments. *Rapid Prototyping J* 2008;14:72–80.
  21. Tam K-MM, Coleman JR, Mueller CT, *et al.* Stress Line Additive Manufacturing (SLAM) for 2.5-D shells. *J IASS* 2016;190:249–259.
  22. Tam K-MM, Coleman JR, Mueller CT, *et al.* Robotics-enabled stress line additive manufacturing. *Proceedings of the 3rd Robotic Fabrication in Architecture, Art and Design (Rob|Arch) Conference*. Cham, CH: Springer, 2016; pp.351–362.
  23. Leary M, Merli L, Torti F, *et al.* Optimal topology for additive manufacture: A method for enabling additive manufacture of support-free optimal structures. *Mater Des* 2014; 63:678–690.
  24. Bablani M, Bagchi A. Quantification of errors in rapid prototyping processes, and determination of preferred orientation of parts. *Transactions of the 23rd North American Manufacturing Research Conference (NAMRC)*. Houghton, MI: NAMRC SME, 2015; pp.319–324.
  25. Leary M, Babae M, Brandt M, *et al.* Feasible build orientations for self-supporting fused deposition manufacture: A novel approach to spacefilling tessellated geometries. *Adv Mater Res* 2013;633:148–168.
  26. Jin GQ, Li WD, Gao L. An adaptive process planning approach of additive manufacturing and manufacturing. *Robot Comput Integr Manuf* 2013;29:23–38.
  27. Han W, Jafari MA, Seyed K. Process speeding up via deposition planning in fused deposition-based layered manufacturing processes. *Addit Manuf* 2003;9: 212–218.
  28. Fonseca J. The loadpath—a way to understand the quality of structures. *J (IASS)* 1997;38:129–135.
  29. Michalatos P, Kaijima S. Eigenshells: Structural patterns on modal forms. In: *Shell Structures for Architecture: Form Finding and Optimization*. Routledge, New York City, NY, 2014; pp.195–210.
  30. Michell AGM. LVII The limits of economy of material in frame-structures. *Philos Mag Ser 6* 1904;47:589–597.
  31. Hemp WS. *Optimum Structures*. Oxford: Oxford University Press, 1973, p.71.
  32. Strang G, Kohn R. Hencky-Prandtl nets and constrained Michell trusses. *Comput Methods Appl Mech Eng* 1983;36: 207–222.
  33. Borelli AP, Schmidt RJ, Sidebottom OM. *Advanced Mechanics of Materials*. Wiley, New York City, NY, 2013.
  34. Jin YA, He Y, Fu JZ. An adaptive tool path generation for fused deposition modeling. *Adv Mater Res* 2013;819: 7–12.
  35. Burns SA. *Recent Advances in Optimal Structural Design*. Institute of the American Society of Civil Engineers, Reston, VA, 2002.
  36. Gibson I, Rosen DW, Stucker B. *Additive Manufacturing Technologies: Rapid Prototyping to Direct Digital Manufacturing*. New York: Springer Science & Business Media, 2010.
  37. Baufeld B, Biest OVD, Gault R. Additive manufacturing of Ti–6Al–4V components by shaped metal deposition: Microstructure and mechanical properties. *Mater Des* 2010; 31:106–111.
  38. Krauss H, Zaeh MF. Investigations on manufacturability and process reliability of selective laser melting. *Phys Procedia* 2013;41:808–815.
  39. Krauss H, Eschey C, Zaeh MF. Thermography for monitoring the selective laser melting process. *Proceedings of the 23rd annual international solid freeform fabrication symposium*. Austin, TX: The University of Texas at Austin, 2012.
  40. Robert McNeel & Associates. Rhinoceros. [www.rhino3d.com](http://www.rhino3d.com) (accessed September 1, 2016).
  41. Rutten D. Back home. In *I eat bugs for breakfast*. <https://ieatbugsforbreakfast.wordpress.com/2013/11/10/back-home/> (accessed September 1, 2016).
  42. Preisinger C. Karamba 3D. [www.karamba3d.com/](http://www.karamba3d.com/) (accessed September 1, 2016).
  43. Flöry S, Schmiedhofer H, Reis M. Rechenraum – Overview. [www.rechenraum.com/en/goat/overview.html](http://www.rechenraum.com/en/goat/overview.html) (accessed September 1, 2016).
  44. MIT License. NLOpt–AbInitio. <http://ab-initio.mit.edu/wiki/index.php/NLOpt> (accessed September 1, 2016).
  45. Tam K-MM, Mueller CT. Stress line generation for structurally performative architectural design. *Proceedings of the 35th Annual Conference of the Association for Computer Aided Design in Architecture (ACADIA): Computational Ecologies: Design in the Anthropocene*. Cincinnati, OH. New York City, NY: Blurb, Incorporated, 2016; pp.95–109.
  46. Halpern AB, Billington DP, Adriaenssens S. The ribbed floor slab systems of Pier Luigi Nervi. *Proceedings of the 54th International Association of Shell and Spatial Structures (IASS) Symposium: Future Visions*. Wroclaw, PL: Wroclaw University of Technology: IASS, 2013.
  47. Mazurek A, Baker W, Tort C. Geometrical aspects of optimum truss like structures. *Struct Multidisc Optim* 2011;45: 231–242.
  48. Rozvany GIN, Bendsoe MP, Kirsch U. Layout optimization of structures. *Appl Mech Rev* 1995;48:41–119.
  49. Achtziger W. Topology optimization of discrete structures: An introduction in view of computational and nonsmooth aspects. In: *Topology Optimization in Structural Mechanics*. Springer Vienna, Wien, AUT; pp.57–100.

50. Adriaenssens S, Richardson JN, Coelbo RF, *et al.* Discrete topology optimization. In: Shell Structures for Architecture: Form Finding and Optimization. Routledge, New York City, NY, 2014; pp.171–180.
51. Stratasys. Dimension 1200es 3D modeling printers | Stratasys. [www.stratasys.com/3d-printers/design-series/dimension-1200es](http://www.stratasys.com/3d-printers/design-series/dimension-1200es) (accessed September 1, 2016).
52. KUKA. KUKA industrial robots – KR 6 R900 sixx (KR AGILUS). [www.kuka-robotics.com/usa/en/products/industrial\\_robots/small\\_robots/kr6\\_r900\\_sixx](http://www.kuka-robotics.com/usa/en/products/industrial_robots/small_robots/kr6_r900_sixx) (accessed September 1, 2016).
53. Signstek. Signstek 3D Reprap printer CNC 40 mm Nema17 1.7A 3.4 V 3400g.cm 2 phase resistance 4 leads electric stepper motor fan motor control. [www.amazon.com/Signstek-Printer-3400g-cm-Resistance-Electric/dp/B00H96G5M0/](http://www.amazon.com/Signstek-Printer-3400g-cm-Resistance-Electric/dp/B00H96G5M0/) (accessed September 1, 2016).
54. Arduino. Arduino–ArduinoBoardUno. [www.arduino.cc/en/Main/ArduinoBoardUno](http://www.arduino.cc/en/Main/ArduinoBoardUno) (accessed September 1, 2016).
55. SparkFun, Schmalz B. EasyDriver – Stepper motor driver. [www.sparkfun.com/products/12779](http://www.sparkfun.com/products/12779) (accessed September 1, 2016).
56. RobotMaster. Robotmaster CAD/CAM for robots (off-line programming). [www.robotmaster.com/en](http://www.robotmaster.com/en) (accessed September 1, 2016).
57. Mastercam. Mastercam CAD/CAM Software > Home. [www.mastercam.com/en-us](http://www.mastercam.com/en-us) (accessed September 1, 2016).
58. Piker D. Kangaroo: Form finding with computational physics. *Architectural Design* 2013;2:136–137.
59. MakerBot. MakerBot 3D printers | MakerBot. [www.makerbot.com/products/3d-printers](http://www.makerbot.com/products/3d-printers) (accessed September 1, 2016).
60. Jacot BP, Caitlin TM. A strain tensor method for three-dimensional Michell structures. *Struct Multidisc Optim* 2016;54:1–11.
61. Huang YJ, Zhang JY, Hu X, Song GX, Liu ZY, Yu L, *et al.* FrameFab: Robotic fabrication of frame shapes. *J ACM Transact Graph* 2016;35:224.

Address correspondence to:

*Kam-Ming Mark Tam*  
*Massachusetts Institute of Technology*  
*77 Massachusetts Avenue*  
*MIT Room 5-418*  
*Cambridge, MA 02139*

*E-mail: kmmt@mit.edu*